Electrochemical Performance of Grids of Lead-acid Batteries made from Pb-0.8%Ca-1.1%Sn Alloys Containing Cu, As and Sb Impurities in the presence of phosphoric acid

H.A. Abd El-Rahman*, A.G. Gad-Allah, S.A. Salih and A. M. Abd El-Wahab
Chemistry Department, Faculty of Science, Cairo University, 12613 Giza, Egypt.

Comportamiento electroquímico de rejillas de baterías de plomo - ácido a base de aleaciones de Pb 0.8% - Ca 1.1% que contienen impurezas de Cu Sn, As y Sb en presencia de ácido fosfórico

Comportament electroquímic de reixes de bateries de plom - àcid a base d'aliatges de Pb 0.8% - Ca 1.1 % que contenen impureses de Cu Sn , As i Sb en presència d'àcid fosfòric

Recibido: 10 de enero de 2013; revisado: 12 de junio de 2013; aceptado: 10 de julio de 2013

RESUMEN

Se estudió el comportamiento electroquímico de rejillas de baterías de plomo-ácido fabricadas a partir de aleaciones Pb 0.8% - Ca 1.1% con impurezas de Sn, Cu, As y Sb a nivel de 0,1 % en peso, en H_2SO_4 4,0M con o sin 0.4 M H_3PO_4. Se encontró que la presencia de impurezas en la aleación o la adición de H_3PO_4 suprimen la tasa de corrosión. El H_3PO_4 aumentó las tasas de evolución tanto de hidrógeno como de oxígeno a elevadas sobretensiones en todas las aleaciones. A excepción de la aleación que contiene Cu, el H_3PO_4 presenta un ligero efecto positivo sobre la formación de PbO_2. La auto-descarga de PbO_2 bajo polarización o en condiciones de circuito abierto aumenta en presencia de H_3PO_4 pero la corrosión de la rejilla positiva se redujo, excepto para la aleación que contiene As. Las aleaciones conteniendo impurezas mostraron una tasa de autodescarga significativamente menor en presencia de H_3PO_4 que en su ausencia. Las medidas de la impedancia permitieron detectar y cuantificar la formación de la capa interna altamente aislante de PbO, debajo de la capa externa de $PbSO_4$, y su transformación al conductor PbO_2, durante la oxidación de aleaciones en condiciones de corriente constante. El H_3PO_4 mejora significativamente la formación de PbO en presencia de impurezas especialmente Sb .

Palabras clave: Aleaciones de Pb-Ca-Sn; baterías de plomo-ácido; plomo reciclado; ácido fosfórico.

SUMMARY

Electrochemical performance of grids of lead-acid Batteries manufactured from Pb-0.8%Ca-1.1%Sn alloys containing Cu, As and Sb impurities at 0.1 wt% level were studied in 4.0 M H_2SO_4 without and with 0.4 M H_3PO_4. The presence of impurities in the alloy or addition of H_3PO_4 was found to suppress the corrosion rate. H_3PO_4 increased the rates of both hydrogen and oxygen evolution reactions at high overpotentials for all alloys. Except for Cu-containing alloy, H_3PO_4 had a slight positive effect on PbO_2 formation. The self-discharge of PbO_2 under polarization or open-circuit conditions increased in the presence of H_3PO_4 but the positive grid corrosion decreased, except for the As-containing alloy. Impurity-containing alloys showed significantly lower self-discharge rate in the presence of H_3PO_4 than in its absence. Impedance measurement was able to detect and quantify the formation of the highly insulating inner PbO layer beneath the outer $PbSO_4$ layer and its transformation to the conducting PbO_2, during the oxidation of alloys under constant current conditions. H_3PO_4 significantly enhanced the formation of PbO in the presence of impurities, especially Sb.

Keywords: Pb-Ca-Sn alloys; lead-acid batteries; recycled lead; phosphoric acid.

RESUM

Es va estudiar el comportament electroquímic de reixes de bateries de plom - àcid fabricades a partir d'aliatges Pb 0.8% - Ca 1.1 % amb impureses de Sn, Cu, As i Sb a nivell de 0,1 % en pes, en H_2SO_4 4,0 M amb o sense 0.4 M H_3PO_4. Es va trobar que tant la presència d'impureses en l'aliatge com l'addició d'H_3PO_4 suprimeixen la taxa de corrosió. L'H_3PO_4 va augmentar les taxes d'evolució tant d'hidrogen com d'oxigen a sobrepressions elevades en tots els aliatges. A excepció de l'aliatge que conté Cu, el H_3PO_4 presenta un lleuger efecte positiu sobre la formació de PbO_2. L'auto-descàrrega de PbO_2 sota polarització o en condicions de circuit obert augmenta en presència d'H_3PO_4 però la corrosió de la reixa positiva es va reduir, excepte per l'aliatge que conté As. Els aliatges que contenen impureses van presentar una taxa d'auto-descàrrega significativament menor en presència d'H_3PO_4 que en la seva absència. Les mesures de la impedància

*Corresponding author: Tel:+202-35676565; Fax: +202-35685799; abdelrahman_hamid@hotmail.com

van permetre detectar i quantificar la formació de la capa interna, altament aïllant, de PbO, sota la capa externa de $PbSO_4$, i la seva transformació a PbO_2 conductor, durant l'oxidació d'aliatges en condicions de corrent constant. El H_3PO_4 millora significativament la formació de PbO en presència d'impureses, especialment Sb.

Paraules clau: Aliatges de Pb-Ca-Sn; bateries de plom-àcid; plom reciclat; àcid fosfòric.

1. INTRODUCTION

In order to improve the performance of lead-acid batteries, several additives to the sulfuric acid electrolyte has been studied, including H_3PO_4 [1-25], H_3BO_3 [26-29] and metal ions [30-39]. H_3PO_4 is by far the most widely studied electrolytic additive for commercial uses in Pb-acid battery and it was found to reduce the sulfation, especially after deep discharge [2-4,7,10], increase the battery cycle life [2-4, 14] and slowing down the self-discharge discharge [13]. The serious disadvantage of addition of H_3PO_4 was a loss in cell capacity [11]. The loss in charge capacity of the battery in the presence of H_3PO_4 decreased as the discharge rate increased [18]. The effect on H_3PO_4 on the efficiency of formation of PbO_2 on positive grid during the charging process was dependent on the charging conditions; some conditions increased the efficiency [6,15] while the others showed the opposite effect [3,5,11,13,22,24]. The presence of H_3PO_4 increased the overpotential of both hydrogen and oxygen evolution reactions [13,16,17]. The effect of binary additives, such as phosphoric and boric acids, on the corrosion of the negative and the positive grids of a lead-acid battery were studied, and the results were explained in terms of H^+ ion transport and the morphological change of the $PbSO_4$ layer [22]. For Pb-Sb alloys, H_3PO_4 decreased the negative effect of antimony in lead alloy [16]. For Pb-1.7%Sb alloys H_3PO_4 suppressed the positive grid corrosion under repeated charging/discharging under constant current [24]. Addition of H_3PO_4 led to deterioration of the insulating properties of the passive layer on Pb-17%Sb in 5M H_2SO_4 by retarding the formation of $PbSO_4$ [25].

Most lead used in the manufacture of grids is provided by the recycling process of lead batteries and other lead products [40-42]. According to ASTM Designation B29-79(84) and Battery Council International (BCI), a tolerance level less than 20 ppm for elemental impurities, such as As, Cu and Sb, in pig lead for the manufacture of grids is recommended. The use of recycled lead with impurity levels above those in the industrial standards seems to be favorable from the environmental and economical points of view.

In the present work, the electrochemical performance of Pb-0.08%Ca-1.1%Sn alloys containing 0.1 wt% of Cu or As or Sb or the three elements combined in 4.0 M H_2SO_4 in the absence and presence of 0.4M H_3PO_4 is studied. Based on the previous studies, it is hoped that the possible harmful effect of impurities may be compensated by the addition of H_3PO_4.

2. EXPERIMENTAL

Disc working electrodes were cut from rods of commercial Pb-Ca-Sn alloys without and with various elemental additions. The composition wt% of Pb-0.8%Ca-1.1%Sn alloy (Alloy I) was as follows: Sn 1.1214, Sb 0.00033, Cu 0.00034, As 0.00019, Ca 0.08279 and Pb 98.7807. Four Impurity-containing alloys were made by the addition of the respective element(s) during the casting; 0.1 wt% As (Alloy II), 0.1 wt% Cu (Alloy III), 0.1 wt% Sb (Alloy IV), and 0.1 wt% As + 0.1 wt% Cu + 0.1 wt% Sb (Alloy V). 2-cm long rod of the alloy was coated with a thin epoxy adhesive (Araldite®, Ciba, Switzerland) and inserted in thick-walled glass tubing with appropriate cross-sectional area. Cross sectional area of the alloy, ca. 0.28 cm^2, was only left to contact the test solution. A stout copper rode was screwed from the other end of the alloy rod to provide the electrical contact of the electrode. The electrodes were mechanically polished with successive grades of emery papers up to 1200 grit, then washed with acetone, double distilled water and finally with a fine tissue so that the surface appeared bright and free from defects. A three-electrode cell was employed in all electrochemical tests. The counter electrode was a platinum sheet of area ca. 2x2 cm^2 and positioned in the cell to face the working disc electrode. The potential of the alloy electrode was measured versus an Hg/Hg_2SO_4/1.0 M H_2SO_4 reference electrode (0.680V vs. SHE). All potentials are given relative to the previously mentioned reference electrode. Chemically ultra-pure 98% H_2SO_4 and 80% H_3PO_4 stocks were used for preparation of solutions by the appropriate dilution using doubly distilled water. All measurements were conducted in unstirred naturally aerated 4.0 M H_2SO_4 acid solutions without and with 0.4 M H_3PO_4 at a constant temperature of 25± 0.2°C. The different electrochemical measurements were carried using the electrochemical system IM6 Zahner electric, Meßtechink, Germany. Impedance was measured at a frequency, f, of 1.0 kHz using an ac potential of 3 mV peak to peak. With the large counter electrode used, the cell impedance was reduced to that of the working electrode and the solution resistance between the working and counter electrodes. The electrode capacitance, C (F) and resistance, R (Ω) values were extracted from the impedance, Z (Ω), and the phase shift angle, θ, of the cell;

$$Z = \sqrt{R^2 + \left(\frac{1}{2f\pi C}\right)^2} \quad \text{and} \quad \tan\theta = \frac{1}{2\pi fRC}.$$

Cyclic voltammetry study was carried out by scanning the electrode potential from -1.9V to 2.0V at a scan rate 50 mV/s. Constant current oxidation/reduction (or in the terminology of the rechargeable batteries: charging/discharging) curves were recorded by applying a cathodic current of 0.54 mA cm^{-2} for 5 minutes to remove any reducible species from the alloy surface, then the current polarity was reversed to oxidize the alloy for 60 minutes. Finally, the current polarity was reversed to reduce the formed PbO_2 on the alloy surface. The reduction continued until the H_2 evolution potential was attained. In the self-discharge tests, the alloys were anodized at 0.54 mA cm^{-2} for 30 minutes, and then the circuit was opened and the open-circuit potential and impedance of the electrode were recorded, until the PbO_2 on alloys was fully self-discharged to $PbSO_4$.

3. RESULTS AND DISCUSSION

3.1. General Corrosion of alloys

Fig. 1 shows Tafel plots for Pb-0.8%Ca-1.1%Sn alloys without and with impurities in 4.0 M H_2SO_4 in the absence

and the presence of 0.4 M H_3PO_4. The shape of Tafel plots is the same for all alloys in the two solutions. The anodic branches show a clear active-passivation transition due the growth of a barrier $PbSO_4$ layer [43,44]. The presence of H_3PO_4 causes a vertical shift in the position of Tafel plots towards less negative potentials. The corrosion current, i_{corr}, the corrosion potential, E_{corr}, and the cathodic and anodic Tafel slopes, b_c & b_a, are given in Table 1. In the absence of H_3PO_4, E_{corr} for alloy I is close to the equilibrium potential, E_{eq}, of the following redox electrode in 4.0 M H_2SO_4 [43,44]:

$$PbSO_4 + 2e \rightleftarrows Pb + SO_4^{2-} \quad ; E_{eq} = -1.04\ V \qquad (1)$$

E_{corr} shifts slightly to less negative values in the presence of the impurities, indicating enhancement of the passivation properties of the naturally formed $PbSO_4$ layer on the corroding alloys. In the presence of H_3PO_4, E_{corr} becomes less negative by 68-57 mV, depending on alloy composition. Two sources for the latter E_{corr} shift are assumed. Firstly, a rise in the solution acidity is expected to shift the equilibrium potentials of the two cathodic processes involved in the corrosion of the alloys, namely, O_2 reduction and H_2 evolution, in the positive direction. Secondly, the phosphate anion acts as a passivity promoter. The presence of H_3PO_4 or impurities in alloys affects the slope of the cathodic branch more significantly than the anodic one. Thus, the corrosion of Pb-0.8%Ca-1.1%Sn alloys is assumed to occur under predominantly cathodic control. Fig. 2 shows the dependence of i_{corr} on alloy type in the absence and the presence of H_3PO_4. Surprisingly, the presence of impurities in alloys leads to a decrease in i_{corr} in the absence and the presence of H_3PO_4. The order of i_{corr} in both solutions is the same: alloy I > alloy III > alloy IV > alloy II > alloy V. The improvement of the corrosion resistance of alloy V (alloy with the three impurities combined) compared to alloys with any individual impurity is attributed to a synergetic effect of impurities that improve the passivation properties of the barrier $PbSO_4$ layer. The percentage corrosion inhibition effect of H_3PO_4, I%, is calculated as follows:

$$I\% = \left(\frac{(i_{corr})_o - (i_{corr})_{H_3PO_4}}{(i_{corr})_o} \right) \times 100 \qquad (2)$$

As can be seen in Fig. 2, I% is practically independent on the alloy composition (48%-55%).

Table 1: *Corrosion data from Tafel plots for Pb-0.8%Ca-1.1%Sn alloys without and with different impurities in 4.0 M H_2SO_4 in the absence and the presence of 0.4 M H_3PO_4 acid. Electrode area = 0.28 cm^{-2}.*

Parameter	I	II	III	IV	V
Absence of H_3PO_4					
E_{corr} / V	-1.026	-1.019	-1.012	-1.014	-1.019
i_{corr} / μA	35.5	17.1	23.6	18.4	14.2
b_c / V	0.926	0.389	0.786	0.538	0.247
b_a / V	0.027	0.018	0.013	0.014	0.017
Presence of H_3PO_4					
E_{corr} / V	-0.958	-0.955	-0.955	-0.951	-0.954
i_{corr} / μA	15.1	8.9	10.6	9.2	7.2
b_c / V	0.378	0.363	0.660	0.386	0.189
b_a / V	0.023	0.023	0.026	0.022	0.022

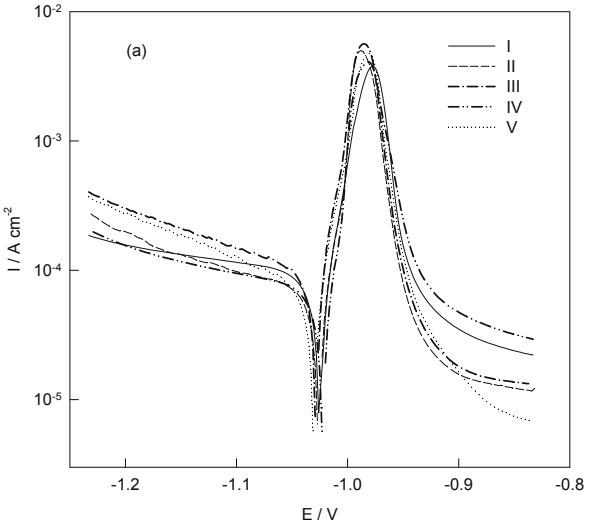

Fig. 1(a)

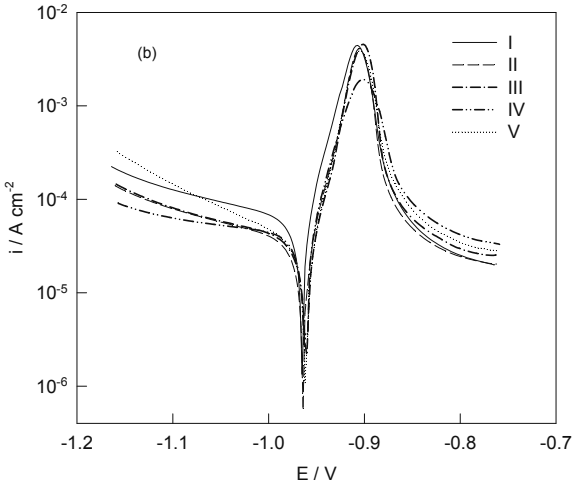

Fig. 1(b)

Fig. 1(a): Tafel plots for Pb-0.8%Ca-1.1%Sn alloys without and with different impurities in 4.0 M H_2SO_4. (b): Tafel plots in the presence of 0.4 M H_3PO_4.

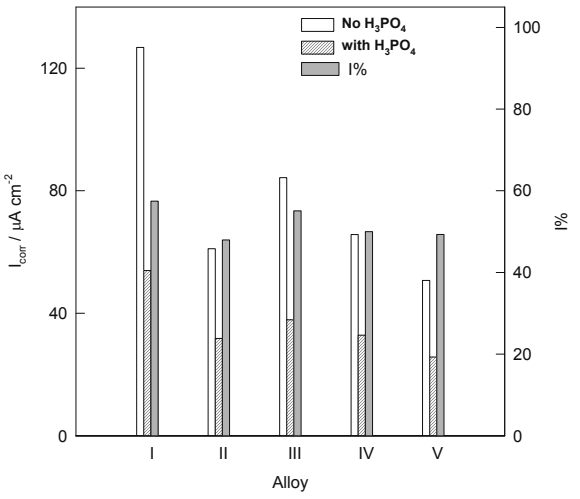

Fig.2. Dependence of the corrosion current, i_{corr}, of Pb-0.8%Ca-1.1%Sn alloys without and with different impurities in 4.0 M H_2SO_4 in the absence and the presence of 0.4 M H_3PO_4.

3.2. Cyclic voltammetry

Fig. 3 shows cyclic voltammograms (CVs) for Pb-0.8%Ca-1.1%Sn alloys without and with impurities in 4.0 M H_2SO_4 in the absence and the presence of 0.4 M H_3PO_4. In one and the same solution, all alloys show the same features with differences in the magnitudes of the redox peaks and a slight shift in the positions of some peaks. No redox peaks related to the impurity element(s) can be detected. CVs reflect only the redox peaks related to Pb component in the alloys and they are similar to those previously reported [45-53]. The significant effects of H_3PO_4 on CVs are: a) All redox peaks shift to more positive (less negative) potentials, b) Significant suppression of peak C_4 occurs and c) The cathodic peak C_1 splits into two peaks (C_1&C_1') and extra peak A" appear.

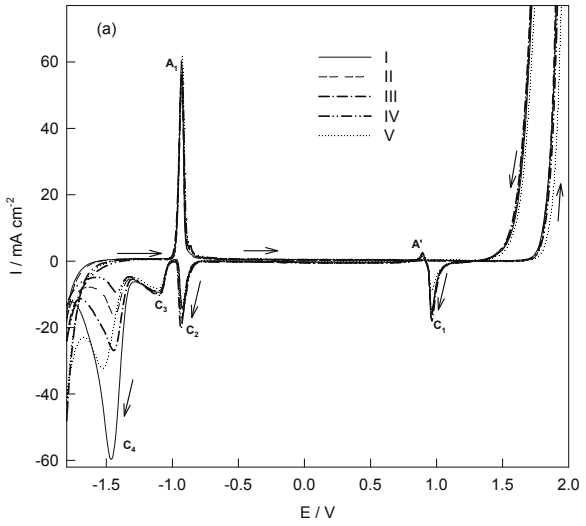

Fig. 3(a)

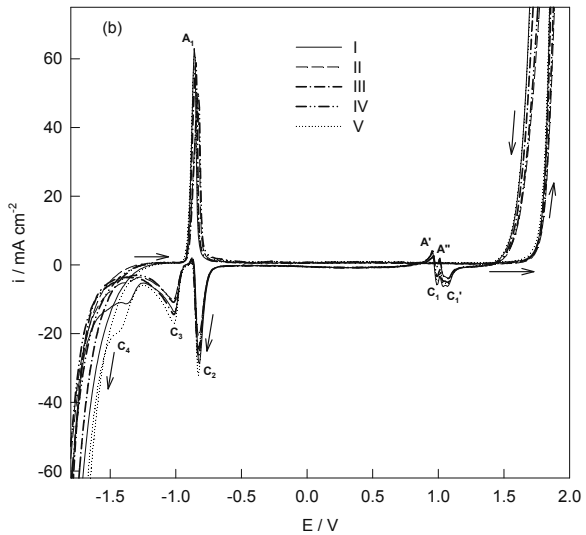

Fig. 3(b)

Fig. 3(a): Cyclic voltammograms of Pb-0.8%Ca-1.1%Sn alloys without and with different impurities in 4.0 M H_2SO_4. (b): Cyclic voltammograms in the presence of 0.4 M H_3PO_4.

The redox peak A_1 is attributed to the formation and growth of a $PbSO_4$ layer on the alloy surface. The passivity region extends after the formation of $PbSO_4$ until the apparent onset of oxygen evolution at ~ 1.7 V. Starting from ~ -0.5V, an insulating PbO layer, beneath $PbSO_4$ layer, is formed. The conducting PbO_2 starts to be formed from Pb^{2+} species at 1.5V with concurrent evolution of O_2. On reversing the potential scan, the formed PbO_2 is reduced in several steps to Pb (C_1-C_4). Peak C_1 is attributed to the electro-reduction of PbO_2 to Pb^{2+} species. The peak potential of C_1 is very close to the reversible potential of the couple $PbO_2/PbSO_4$. When PbO_2 is reduced to $PbSO_4$, a large increase of the molar volume is expected and, as a result, the surface cracks, exposing the bare metal. These parts of the bare surface are then oxidized in an "anodic excursion" peak A' [36,50]. The presence of H_3PO_4 seems to favor the formation of two kinds of PbO_2 (possibly α-PbO_2 and β-PbO_2) that are reduced to $PbSO_4$ in two separate peaks C_1 and C_1'. The anodic excursion Peaks A' and A" appear as a result of peaks C_1 and C_1'. Peak C_2 is attributed to the reduction of PbO to Pb and peaks C_3 and C_4 are connected to the reduction of small and large crystals of $PbSO_4$ to Pb [48]. The peak potentials of C_2-C_4 occur at significantly more negative potentials than the reversible potentials for the couples $PbOPbSO_4$/Pb and $PbSO_4$/Pb, respectively. This is probably due to the insulating nature of these compounds that leads to large ohmic drop and hence, the peak potentials shift to more negative potentials.

It is obvious that the amount of charge consumed in Pb^{4+} to Pb^{2+} reduction (peak C_1) is much lower than the charge consumed in Pb^{2+} to Pb (peaks C_2-C_4). This is mainly attributed to the strong contribution of the self-discharge of PbO_2 with the underlying Pb in the alloys [21,22, 28]. Also, the processes at A' and A" peaks add more Pb^{2+} species. The self-discharge spontaneously occurs according to the following comproportionation reaction [24,25,43,44]:

$$PbO_2 + Pb + 2H_2SO_4 \rightarrow 2PbSO_4 + 2H_2O \quad (3)$$

H_3PO_4 significantly suppresses peak C_4 for all alloys, especially for alloy I. This indicates that H_3PO_4 suppress the formation of large crystals of $PbSO_4$. In the absence of H_3PO_4, the amount of large crystal $PbSO_4$ decreases in the order: Alloy I > Alloy V > Alloy III > Alloy II > Alloy IV. In the Presence of H_3PO_4, the amount of large crystal $PbSO_4$ decreases in the order: Alloy V > Alloy I > Alloy II > Alloy III > Alloy IV. Among the impurity-containing alloys, the alloy with the three impurities (alloy V) forms the largest amount of large crystal $PbSO_4$.

3.3. Hydrogen and oxygen evolution reactions

Fig 4 shows cathodic Tafel polarization curves for the hydrogen evolution reaction (HER) on Pb-0.8%Ca-1.1%Sn alloys in 4.0 M H_2SO_4 in the absence and the presence of 0.4 M H_3PO_4. In the absence of H_3PO_4, a linear Tafel plot for HER on alloy I could only be observed at overpotentials more negative than -1.6V while the presence of impurities in alloys or H_3PO_4 it is possible to see linear Tafel plots at lower cathodic overpotentials. The Tafel slope for HER significantly depends on the alloy composition in the absence of H_3PO_4 (0.136-0.230 V/decade), but it is higher and practically independent on the alloy type in the presence of H_3PO_4 (0.298 - 0.322 V/decade).

The kinetics of oxygen evolution reaction (OER) is more difficult to deduce due to the concurrent PbO_2 formation during the OER at sufficiently high anodic potentials. A simple procedure was used in the present work to suppress PbO_2 formation by holding the potential at 1.9 V for 10 minutes before scanning the potential in the cathodic direction till 1.4V. As can be seen in Fig. 5, linear

Tafel plots over more than two decades of current for OER in the absence of H_3PO_4 could be obtained, though the linearity region in the presence of H_3PO_4 is shorter. The fact that the Tafel plots are almost parallel indicates that the OER mechanism is independent on the alloy type. The Tafel slope for OER in the absence of H_3PO_4 (0.170 - 0.179 V/decade) is higher than in the presence of H_3PO_4 (0.128 - 0.141 V/decade).

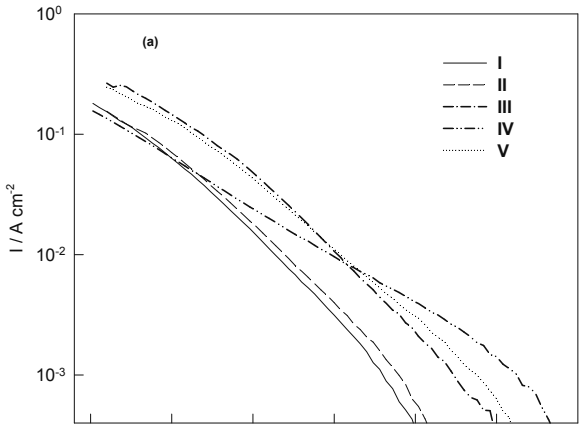

Fig. 4(a)

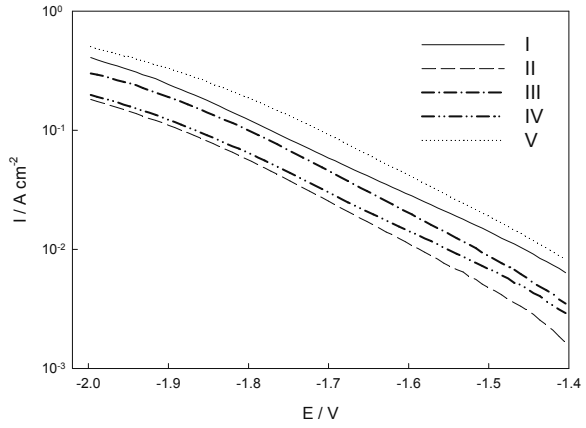

Fig. 4(b)

Fig. 4(a): Cathodic polarization curves of the hydrogen evolution reaction (HER) on Pb-0.8%Ca-1.1%Sn alloys without and with different impurities in 4.0 M H_2SO_4. (b): Cathodic polarization curves of HER in the presence of 0.4 M H_3PO_4.

In the constant current charging process of a battery and as the potential of the full charge capacity is reached, water decomposition to H_2 gas at the negative grid and O_2 gas at the positive grid becomes the prevailing process. Without the proper recombination of H_2 and O_2 gases to water, as in good valve-regulated lead-acid batteries (VRLAB), water loss problems are expected to occur. Alloys with high overpotentials for HER and OER, at a specific current, are desirable to avoid water and energy losses. Alternatively, alloys with lower currents, at constant and sufficiently high overpotential, are preferred. Fig. 6 shows the dependence of HER at -1.9V and OER at 1.9V on the alloy type in the absence and the presence of H_3PO_4. It is clear that H_3PO_4 increases the rates of OER and HER for all alloys. Hence, the addition of H_3PO_4 should be expected to increase the water loss problems, where Alloys I and V show the worst HER and ORE performances compared to their performances in the absence of H_3PO_4.

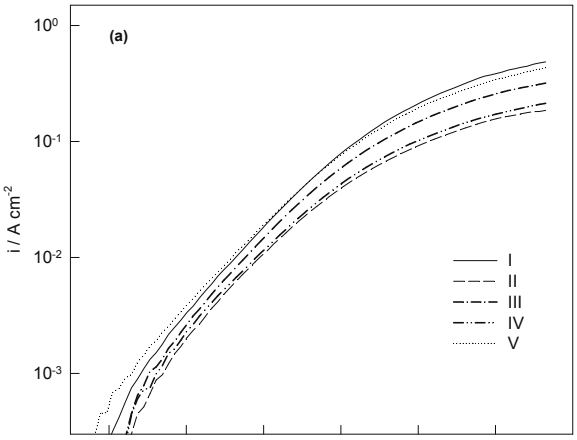

Fig. 5(a)

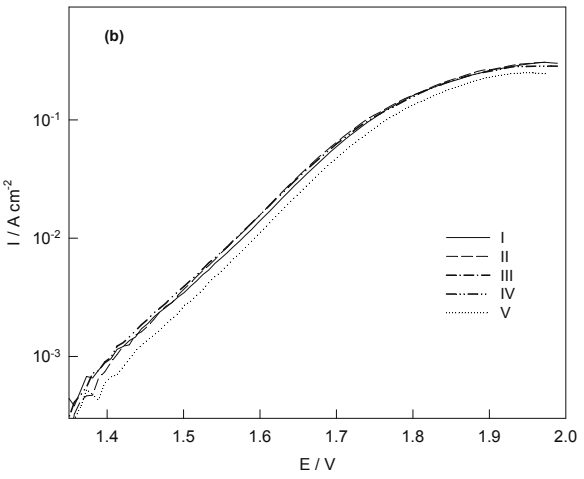

Fig. 5(b)

Fig. 5(a): Anodic polarization curves of the oxygen evolution reaction (OER) on Pb-0.8%Ca-1.1%Sn alloys without and with different impurities in 4.0 M H_2SO_4. (b): Anodic polarization curves of OER in the presence of 0.4 M H_3PO_4.

3.4. Constant current charging/discharging

Fig. 7 shows instantaneous E, C and R curves during the anodic (charging)/cathodic (discharging) polarization of alloy I at 0.54 mA cm^{-2} in 4.0 M H_2SO_4 in the absence and the presence of 0.4 M H_3PO_4. The curves for the rest of alloys showed the same features and the corresponding curves for alloy V, as a representative example, are shown in Fig. 8. C is represented on a logarithmic scale for a better resolution due to the large change in C during the charging/discharging processes. The fact that the time of reduction is higher (> 80 min.) than the oxidation time (60 min.) indicates that new reducible species are involved in the reduction, beside the oxidation products, mainly PbO_2. The nature of these new species will be discussed later. The main features of polarization curves in the in the absence and presence of H_3PO_4 are the same.

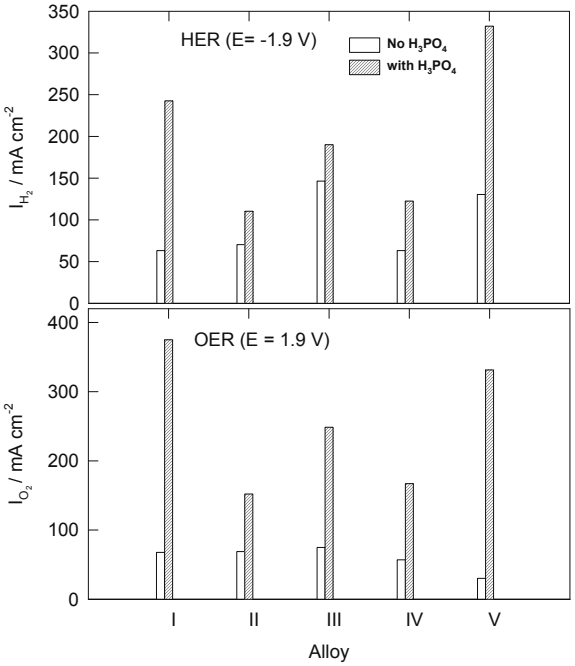

Fig. 6: Currents of HER at -1.9V and OER at 1.9Vfor Pb-0.8%Ca-1.1%Sn alloys without and with different impurities. Details are shown in Figs. 4&5.

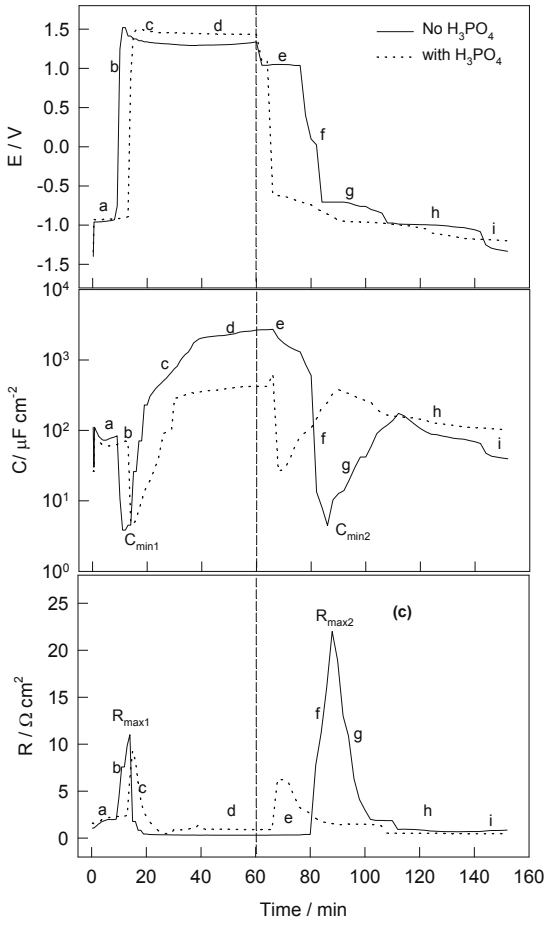

Fig. 7: Instantaneous potential, E, capacitance, C, and resistance, R, during the galvanostatic oxidation/reduction of alloy I at 0.54 mA cm^{-2} in 4.0 M H_2SO_4 in the absence and the presence of 0.4 M H_3PO_4. The vertical dashed line refers to the start of the reduction.

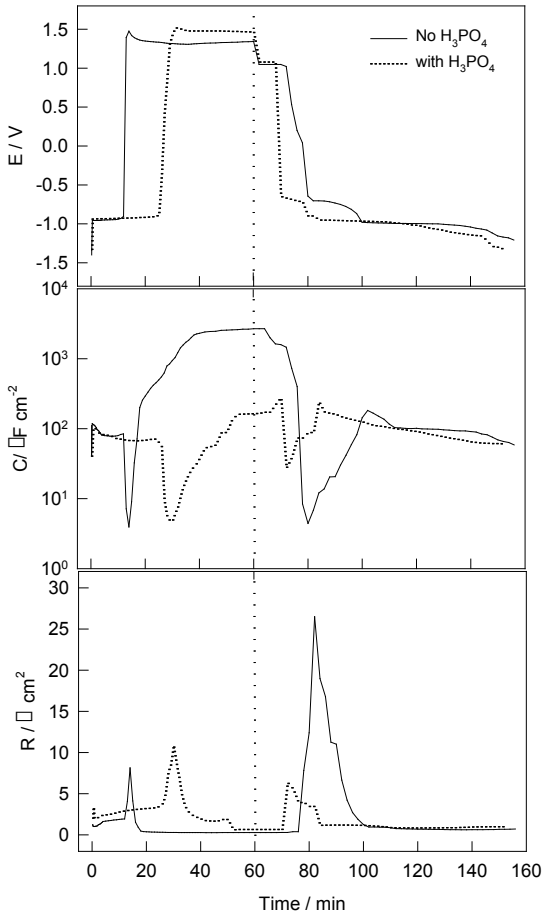

Fig. 8: Instantaneous potential, E, capacitance, C, and resistance, R, during the galvanostatic oxidation/reduction of alloy V at 0.54 mA cm^{-2} in 4.0 M H_2SO_4 in the absence and the presence of 0.4 M H_3PO_4 acid. The vertical dotted line refers to the start of the reduction.

As can be seen in Fig. 7, the oxidation process involves three distinct regions (a), (b) and (c) and (d):

- In region (a), a potential arrest at -0.96 V is seen. It shifts to -0.93 V in the presence of H_3PO_4. It is slightly more positive than the equilibrium potential of the redox Pb/$PbSO_4$ [24,40,41]. In this region, C decreases slightly to a minimum, and then it increases slowly. Concurrently, R increases with time to reach quasi-stationary values by the end of this region. The results indicate the growth of the thin $PbSO_4$ film on the alloy surface. The time of this region is used for the calculation of the amount of charge consumed in formation of $PbSO_4$, $Q^f_{PbSO_4}$.
- The following region (b) is characterized by a sharp increase in E from -0.95V to 1.5V. A corresponding sharp decrease in C to a minimum, C_{min1} (< 1 μF cm^{-2}), and a sharp increase in R to a maximum, R_{min1}, occur. These C and R changes are attributed to the formation of a highly insulating inner PbO film beneath the $PbSO_4$ layer [24,49]. The formation of inner PbO layer is possible because $PbSO_4$ film acted a barrier to retard the diffusion of H_2SO_4 into the growing film. As consequence, pH increases at the alloy/$PbSO_4$ interface and the formation of PbO becomes favorable. The time needed to reach C_{min1} or R_{max1} is the same and

it is used to in the calculation of the amount of charge consumed in the formation of PbO, Q^{f}_{PbO}.

- In region (c), potential decreases slowly to more or less stationary values. At the same time, C starts to increase very sharply (several mF cm^{-2}) and R decreases to the solution resistance. This clearly indicates the transformation of PbO to the conducting PbO_2 and growth of PbO_2.
- In region (d), potential increases slightly and C increases, but with a slower rate than in region (C), due to the strong contribution of OER. It is interesting to note that C continues to increase even after switching the current polarity (after 60 min. of oxidation) to start the reduction of PbO_2. This behavior is attributed to a change in the dielectric properties of PbO_2 layer as a result of the concurrent OER and involvement of O_2 species in the growing PbO_2 layer [24].

Reduction (discharge) process involves five regions (e), (f), (g), (h) and (i):

- In region (e), a potential arrest at 1.0V is seen which is close to the equilibrium potential of the redox $PbSO_4$/PbO_2 in 4.0 M H_2SO_4. Thus, the electrochemical process in region (e) is the electro-reduction of PbO_2 to $PbSO_4$ [24,43]. During this stage of reduction, C increases in the initial stage of the reduction to a maximum, and then it decreases most probably due to the electro-transformation of the conducting PbO_2 (higher dielectric constant material) into the insulating $PbSO_4$(lower dielectric constant material).
- The region (f) shows sharp decreases in potential and C and a sharp increase of R. This region ends with a minimum C, C_{min2}, and a maximum R, R_{max2}, This region signifies the formation of an inner insulating PbO layer beneath $PbSO_4$ by the electro-reduction of the remaining PbO_2 at the alloy/film interface. The time sum for regions (e) & (f) is used in the calculation of the amount of charge consumed in the reduction of PbO_2, $Q^{r}_{PbO_2}$.
- In region (g), the potential arrest(s) at ~ -0.7 V (sometimes ill-definite) is (are) attributed to the reduction of the basic lead sulphates, PbO·$PbSO_4$ and 3PbO·$PbSO_4$, to Pb according to the following processes [24,43]:

$$3PbOPbSO_4 + 6H^+ + 8e \rightleftarrows 4Pb + SO_4^{2-} + 4H_2O; \quad E_{eq} = -0.66\ V \qquad (4)$$

$$PbOPbSO_4 + 2H^+ + 4e \rightleftarrows 2Pb + SO_4^{2-} + H_2O; \quad E_{eq} = -0.8\ V \qquad (5)$$

Considerable increase in C and a decrease in R are noticed in this region and they are attributed to the transformation of the insulting PbO and $PbSO_4$ into the conducting Pb.

- In region (h), $PbSO_4$ is reduced to Pb with a slow decrease in C. The capacitance behavior in this region reflects two opposite effects; a decrease in the surface coverage with $PbSO_4$ and an increase in the interfacial acid concentration. The times of regions (g) & (h) are used in the calculation of the amounts of charges consumed in the reduction of the basic lead sulphates, Q^{r}_{BLS} and $PbSO_4$, $Q^{r}_{PbSO_4}$, respectively.
- By the end of region (h), the alloy surface is assumed to be free from any reducible lead products and potential shifts to a more negative potential (~ -1.3V) where H_2 evolves, region (i). In this region, there is a decrease in C and a slight increase in R, probably due to the H_2 bubbles evolved.

Table 2: *Charge densities consumed in the various redox processes in the charging/discharging of Pb-0.8%Ca-1.1%Sn alloys at 0.54 mA cm^{-2} in 4.0 M H_2SO_4 in the absence and presence of 0.4 M H_3PO_4.*

Charge	I	II	III	IV	V
Absence of H_3PO_4					
$Q^{f}_{PbSO_4}$ / C cm^{-2}	0.194	0.151	0.324	0.259	0.259
Q^{f}_{PbO} / C cm^{-2}	0.086	0.065	0.043	0.065	0.043
$Q^{r}_{PbO_2}$ / C cm^{-2}	0.497	0.346	0.346	0.259	0.410
Q^{r}_{BLS} / C cm^{-2}	0.518	0.605	0.303	0.626	0.432
$Q^{r}_{PbSO_4}$ / C cm^{-2}	0.734	0.972	1.188	0.994	1.080
$Q^{f}_{PbO_2}$ / C cm^{-2}	1.751	1.920	1.842	1.881	1.922
Presence of H_3PO_4					
$Q^{f}_{PbSO_4}$ / C cm^{-2}	0.356	0.389	0.486	0.162	0.745
Q^{f}_{PbO} / C cm^{-2}	0.130	0.130	0.097	0.259	0.259
$Q^{r}_{PbO_2}$ / C cm^{-2}	0.130	0.097	0.197	0.113	0.194
$Q^{r}_{PbOPbSO_4}$ / C cm^{-2}	0.583	0.583	0.324	0.842	0.194
$Q^{r}_{PbSO_4}$ / C cm^{-2}	0.713	1.129	1.361	0.713	1.296
$Q^{f}_{PbO_2}$ / C cm^{-2}	1.426	1.906	1.882	1.782	1.684

Table 2 summarizes the dependence of the charge consumed in the oxidation and the reduction processes in the absence and the presence of H_3PO_4 on alloy type. The effect of H_3PO_4 on the formation of the various compounds in the oxidation steps was expressed as percentage of the relative amount of substance, RAS%, according to the relation:

$$RAS\% = \left(\frac{(Q^{f}_{substance})_o - (Q^{f}_{substance})_{H_3PO_4}}{(Q^{f}_{substance})_o} \right) \times 100 \qquad (6)$$

Where $(Q^{f}_{substance})_o$ and $(Q^{f}_{substance})_{H_3PO_4}$ are the amounts of the substances in the absence and the presence of H_3PO_4, respectively.

The large difference between $Q^{r}_{PbO_2}$ and Q^{r}_{BLS} + $Q^{r}_{PbSO_4}$ (Table 2) is attributed to the self-discharge of PbO_2 according to process (3). The charge loss due to the self-discharge, Q_{SD}, was estimated according to the relation:

$$Q_{SD} = 0.5\left(Q^{r}_{BLS} + Q^{r}_{PbSO_4}\right) - Q^{r}_{PbO_2} \qquad (7)$$

The charge consumed in formation of PbO_2, Q^{f}_{PbO2}, was calculated according to the relation:

$$Q^{f}_{PbO_2} = 2\left(Q^{r}_{PbO_2} + Q_{SD}\right) \qquad (8)$$

The percentage of the self-discharge during the reduction, SD_r, was determined as follows:

$$SD_r\% = \left(Q_{SD} / 0.5Q^{f}_{PbO_2}\right) \times 100 \qquad (9)$$

PbO_2 is considered the final corrosion product in the oxidation (charging) process of alloys and the rate of the

positive grid corrosion, PG_{corr} (g cm^{-2} h^{-1}), was calculated from $Q^{f}_{PbO_2}$ with the aid of Faraday's laws as follows:

$$PG_{corr} = Q^{f}_{PbO_2} \times 207.19/4F \quad (10)$$

Where the value 207.19 is the atomic mass of Pb. The effect of H_3PO_4 on the parameters $SD_r\%$ and PG_{corr} was expressed as a percentage of the relative parameter, RP% according to the relation:

$$RP\% = \left(\frac{(RP)_o - (RP)_{H_3PO_4}}{(RP)_o} \right) \times 100 \quad (11)$$

Where $(RP)_o$ and $(RP)_{H_3PO_4}$ are parameters in the absence and the presence of H_3PO_4.

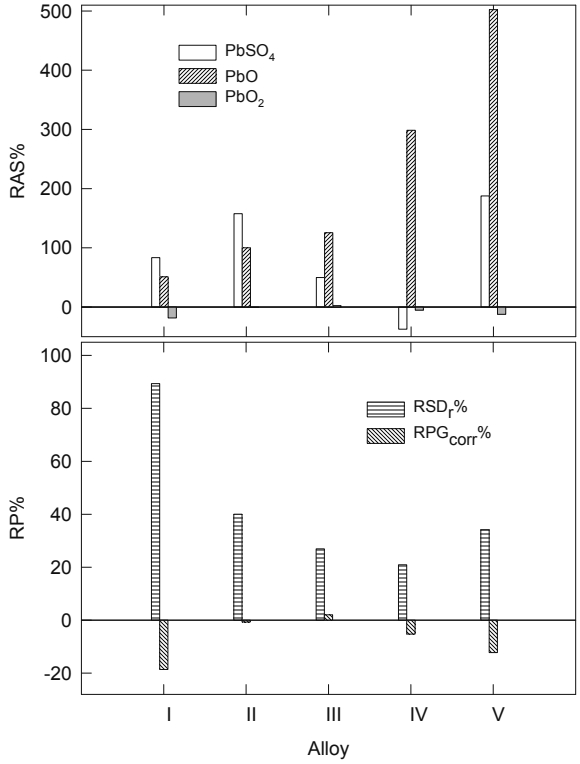

Fig. 9: Dependence of the relative change due to H_3PO_4 in amounts of $PbSO_4$, PbO and PbO_2 formed during constant current oxidation of Pb-0.8%Ca-1.1%Sn alloys (Upper) and in the self-discharge during polarization, RSD_p, and the positive grid corrosion, PG_{corr} (Lower) on alloy type.

Fig. 9 shows the dependence of RAS% and RP% on the alloy type. The presence of H_3PO_4 leads to:

- An increase in the amount of PbO formed during the charging of all alloys, especially in the presence of either Sb (alloy IV) or the three impurities (alloy V).
- An increase in the amount of $PbSO_4$ formed during the charging process of all alloys, except for the alloy containing Sb (alloy IV).
- A slight negative effect on the PbO_2 formation during the charging of all alloys, except alloy containing Cu (alloy III).
- An increase in $RSD_r\%$ for all alloys but the extent is lower in the presence of the impurities.
- A slight decrease in $RPG_{corr}\%$ for all alloys except for a very slight increase in case of the alloy containing As (alloy II).

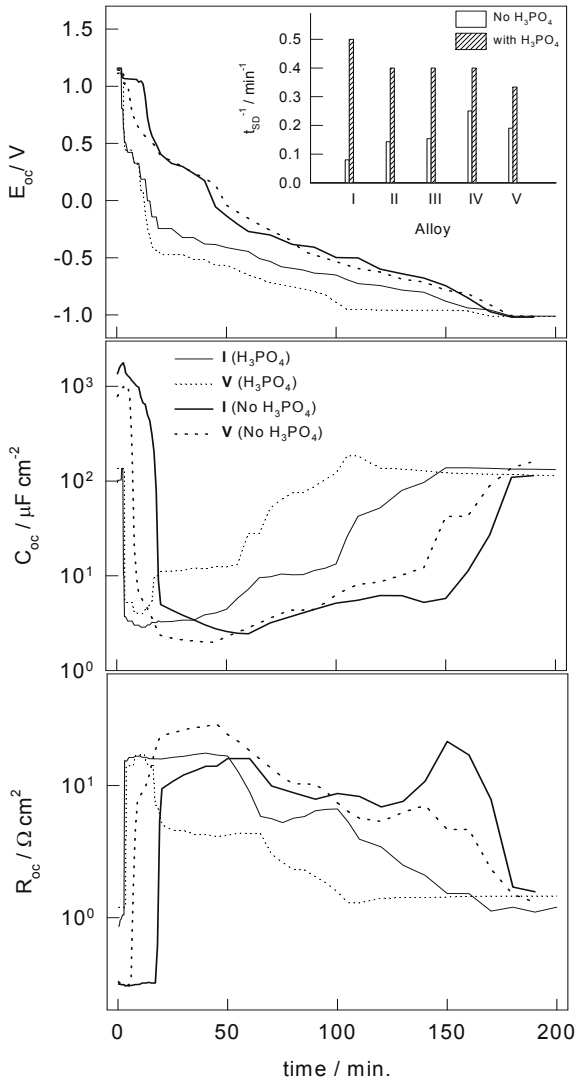

Fig. 10: Instantaneous open-circuit potential, E_{oc}, capacitance, C_{oc}, and resistance, R_{oc} during the self-discharge of alloys I and V in 4.0 M H_2SO_4 + 0.4 H_3PO_4 under open-circuit conditions. The alloys were pre-oxidized at 0.54 mA for 30 minutes. Inset in the upper part: Dependence of the self-discharge rate, t_{SD}^{-1}, on alloy type.

3.5. Self-discharge under open-circuit conditions

Fig. 10 shows the variation of the open-circuit potential, E_{oc}, capacitance, C_{oc}, and resistance, R_{oc}, of the pre-oxidized alloys I and V with time in 4.0 M H_2SO_4 in the absence and presence of 0.4 M H_3PO_4. The alloys are pre-oxidized (charged) at 0.54 mA for 30 minutes. The self-discharge curves for the rest of alloys showed the same features of curves in Fig. 10. As can be seen, about 3 hours are needed for the full self-discharge of the PbO_2 (E_{oc} = ~1.2 V) to $PbSO_4$ (E_{oc} = ~ -1.0 V). At the beginning, E_{oc} stays almost invariant with time for a period of time that depends on the alloy type and the presence or the absence of H_3PO_4. Then, it starts to rapidly decay to less positive values. A substantial decrease in C and an increase in R are seen during the rapid E_{oc} decay. These variations are attributed to the self-discharge of the inner PbO_2 layer to PbO via the reaction of inner PbO_2 layer with the underlying Pb on the alloy surface according to the process:

$$PbO_2 + Pb \rightleftarrows 2PbO \quad (12)$$

At ~ -0.3V, E_{oc} slows down and concurrently an irregular increase in C and an irregular decrease in R can be seen. The latter variations in C and R are attributed to the chemical transformation of the inner PbO layer into $PbSO_4$ as a result of the diffusion of H_2SO_4 from solution into the passive film [49]:

$$PbO + H_2SO_4 \rightleftarrows PbSO_4 + H_2O \quad (13)$$

The reciprocal of the time required to start the rapid decay from E_{oc} = 1.0V, t_{SD}^{-1}, was taken as a measure for the self-discharge rate of the alloy. Inset of Fig. 11 shows that the presence of H_3PO_4 increases the self-discharge rate of all alloys. However, the effect of H_3PO_4 is more pronounced for alloy I than the alloys containing the impurities.

CONCLUSION

- Corrosion of Pb-0.8%Ca-1.1%Sn alloys is assumed to occur under predominantly cathodic control in the absence and the presence of H_3PO_4. The presence of impurities in alloys or H_3PO_4 in solution lead to a decrease in i_{corr} and the three impurities combined showed the best corrosion resistance.
- In cyclic voltammetry, H_3PO_4 shifts all redox peaks to more positive potentials, significantly suppresses the cathodic peak of large crystal $PbSO_4$ and leads to the splitting of the reduction peak of PbO_2 to $PbSO_4$.
- H_3PO_4 increases the rates of OER and HER for all alloys, especially for the alloy without impurities and the alloy with the three impurities combined.
- In the constant current charging/discharging tests, H_3PO_4 decreases slightly the amount of PbO_2 for all alloys except for the copper containing alloy. Although impurities deteriorate the positive grid corrosion, H_3PO_4 slightly decreases this corrosion form for all alloys, except for arsenic containing alloy.
- The presence of the H_3PO_4 increases the self-discharge of PbO_2 either under polarization conditions or under open-circuit conditions, though the extent of this negative effect is lower for alloys with impurities.

REFERENCES

1. J. Burbank, J. Electrochem. Soc. 111, 1112 (1964).
2. S. Tudor, A. Weisstuch, S.H. Davang, Electrochem. Technol.,3, 90 (1965).
3. S. Tudor, A. Weisstuch, S.H. Davang, Electrochem. Technol.,4, 406 (1966).
4. S. Tudor, A. Weisstuch, S.H. Davang, Electrochem. Technol., 5, 21 (1967).
5. H.A. Laitinen, N. Walkins, Anal. Chem.,47, 1353 (1975).
6. W. Visscher, J. Power Sources,1, 257 (1976/77).
7. K.R. Bullock, D.H. McClelland, J. Electrochem. Soc.,124, 1478 (1977).
8. B.K. Mahato, J. Electrochem. Soc.,126, 369 (1979).
9. K.R. Bullock, J. Electrochem. Soc.,126, 1848 (1979).
10. K.R. Bullock, J. Electrochem. Soc.,126, 360 (1979).
11. S. Stemberg, A. Mateescu, V. Branzoi, L. Apateanu, Electrochim. Acta, 32, 349 (1987).
12. E. Voss, J. Power Sources, 24,171 (1988).
13. S. Sternberg, V. Branzoi, L. Apateanu, J. Power Sources, 30, 177 (1990).
14. J. Garche, H. Doring, K. Wiesener, J. Power Sources, 33, 213 (1991).
15. H. Doring, K. Wiesener, J. Garche, Pl. Fischer, J. Power Sources,38, 261 (1992).
16. S. Venugopalan, J. Power Sources, 46, 1 (1993).
17. S. Venugopalan, J. Power Sources, 48, 371 (1994).
18. E. Meissner, J. Power Sources,67, 135 (1997).
19. A. Bhattacharya, I. N. Basumallick, J. Power Sources,113, 382 (2003).
20. I. Paleskaa, R. Pruszkowska-Drachala, J. Kotowskia, A. Dziudzia, J.D. Milewskic, M. Kopczykc, A. Czerwinskia, J. Power Sources,113, 308 (2003).
21. S. Li, H.Y. Chen, M.C. Tang, W.W. Wei, Z.W. Xia, Y.M. Wu, W.S. Li, X. Jiang, J. Power Sources ,158, 914 (2006).
22. K. Saminathan, N. Jayaprakash, B. Rajeswari, T. Vasudevan, Journal of Power Sources, 160, 1410 (2006).
23. S. Li a, H.Y. Chena, M.C. Tang b, W.W. Weib, Z.W. Xia b, Y.M. Wu b, W.S. Li a, X. Jiang, J. of Power Sources 158, 914 (2006).
24. H.A. Abd El-Rahman, S.A. Salih and A. M. Abd El-Wahab, Mat.-wiss.Werkstofftech., 42, 784 (2011).
25. A. Abd El-Rahman, S.A. Salih, and A. M. Abd El-Wahab, Journal of Electrochemical Science and Technology, 2, 76 (2011).
26. Yu.A. Zinchenko, O.L. Aleksandrova, M.R. Biegul, A.1. Petrukhova and V.D. Bar'Sukov, Tovarnye Znaki, 48, 1194 (1971).
27. I.M. Ismail, A.H. El Abd, Chem. Age India, 34, 393 (1983).
28. W.A. Badawy, S.S. El-Egamy, J. Power Sources, 55, 11 (1995).
29. B.K. Mahato, W.H. Tiedemann, J. Electrochem. Soc., 130, 2139 (1983).
30. M. Maja, N. Penazzi, J. Power Sources, 22, 1 (1988).
31. H. Sanchez, Y. Meas, I. Gonzalez, M.A. Quiroz, J. Power Sources, 32, 43 (1990).
32. D. Pavlov, J. Power Sources,33, 221 (1991).
33. D. Pavlov, A. Dakhouche, T. Rogachev, J. Power Sources, 42, 71 (1993).
34. D. Pavlov, J. Power Sources , 46, 171 (1993).
35. L.T. Lam, J.D. Douglas, R. Pilling, D.A.J. Rand, J. Power Sources, 48, 219 (1994).
36. K. Mc Gregor, J. Power Sources,59, 31 (1996).
37. T. Rogachev, D. Pavlov, J. Power Sources, 64, 51 (1997).
38. N. Chahmanaa, M. Matrakovab, L. Zerroual, D. Pavlov, J. Power Sources, 191, 51 (2009).
39. N. Chahmana, L. Zerroual, M. Matrakova, J. Power Sources, 191, 144 (2009).
40. M. Stevenson, Recycling, Lead-Acid Batteries: overview, Encyclopedia of Electrochemical Power Sources, pp. 165-178 (2009).
41. S. Prolich and D. Sewig, J. Power Sources, 57, 27 (1995).
42. T. W. Ellis and A. H. Mirza, J. Power Sources, 195, 4525 (2010).
43. A.G. Gad-Allah, H.A. Abd El-Rahman, S.A. Salih, M. Abd El-Galil, J Appl. Electrochem., 25, 682 (1995).
44. A.G. Gad-Allah, H.A. Abd El-Rahman, S.A. Salih, M. Abd El-Galil, J Appl. Electrochem., 22, 571 (1997).

45. F. E. varela, E. N. Cordoro and J. R. Vilche, Electrochim. Acta, 40, 1183 (1995).
46. Y. Yamamoto, M. Matsuka, M. Kimoto, M. Uemura and C. Iwakura, Electrochim. Acta, 41, 439 (1996).
47. E.N. Codaro, J.R. Vilche, Electrochim. Acta, 42, 549, 979 (1997).
48. Y. Guo, M. Wu and S. Hua, J Power Sources, 64, 65 (1997).
49. Y. Guo, Z. Wei and S. Hua, Electrochim. Acta, 42, 979 (1997) .
50. A. Czerwinski, M. Zelazowska, M. Grden, K. Kuc, J.D. Milewski, A. Nowacki, G. Wojcik, M. Kopczyk , J. Power Sources, 85, 49. (2000)
51. Q. Sun, Y. Guo, J. Electroanal. Chem., 493, 123 (2000).
52. E. Rocca, J. Steinmetz, J. Electroanal. Chem., 543, 153 (2003).
53. M. Metikos-Hukovic, R. Babic, S. Brinic, J. Power Sources,157, 563 (2006).